CHAPTER

MATHEMATICAL MODELING OF HARDWARE IMPAIRMENTS

4

As Gordon Moore accurately predicted more than 50 years ago [19], the number of transistors in a dense integrated circuit doubles approximately every two years. In retrospect we have seen the industry follow Moore's observation and it is clear that this development has paved the way for high speed digital communication systems with highly integrated radio transceivers. This development has led to a movement of the border between analog and digital domains in which we today see radio transceivers which are becoming predominantly digital in design.

Through the development of high speed, real-time processing, techniques for compensating imperfections in analog hardware are today commonly used extensively due to stringent requirements imposed by the physical layer design. At the basis for any effective compensation algorithm lies a behavioral model mimicking the behavior of an imperfect analog component. Algorithms such as DPD for linearization of power amplifiers and phase-noise tracking all rely on accurate behavioral modeling in order to perform accurate mitigation.

One aspect that underlines the importance of radio hardware impairment modeling is the constant increase of throughput which is enabled by either using large channel bandwidths at millimeter-wave frequencies or by increasing the spectral efficiency by a denser modulation format and spatial multiplexing. In both of these directions, new challenges face the radio hardware design and the importance of accurate impairment models grows. One particular technology component important for 5G is that of multiantenna techniques such as massive MU-MIMO for spatially multiplex users at sub-6 GHz, along with different methods for analog or hybrid beam-forming techniques aimed toward higher frequencies in the millimeter-wave frequency bands. In both of these areas, impairment models may not only serve as a basis for advanced compensation mechanisms, but also provide valuable insights in how the impairments behave in the spatial domain.

Impairment modeling has also in recent years gained interest from researchers working in the field of communication systems design. Until now, however, may of the models used have been oversimplified for analytical convenience, [3]. However, under some circumstances these simplified models, which are quite often just additive and independent noise, may provide misguiding insights as they do not accurately represent the statistical properties of the impairments, [17].

Conventional behavioral models are however lacking in this aspect as they require time-domain signals, often oversampled. Since knowing the statistical properties of the distortion suffices for conventional link-level analysis which often relies on asymptotics, alternative approaches may be considered in which the impairments are modeled as a correlated noise process. As will be shown in this chapter, the properties of this noise process may be determined using parameterizations of the corresponding behavioral model and knowledge of the transmit covariance.

On a final note—the underlying mathematics behind most common behavioral models used to capture effects of hardware impairments may be more than a century old but, as we will illustrate in

5G Physical Layer. https://doi.org/10.1016/B978-0-12-814578-4.00009-6

this chapter, the modeling work is still evolving in order to support the design of future radio access technologies and advanced antenna systems.

In this chapter, we will overview and discuss the current state-of-the-art in behavioral modeling of some important radio hardware subsystems. We will start with the power amplifier and the Volterra series commonly used to model their behavior. We will also discuss a novel extension used to model power amplifiers in antenna systems which may be under the influence of mutual coupling, something which is becoming increasingly important with the current drive toward compact antenna arrays operating at millimeter-wave frequencies. This is followed by a discussion on oscillator phase noise and the underlying Wiener process commonly used for modeling. We then move on to discuss quantization noise in data converters and how to model the granular noise from the quantization process and the distortion arising from clipping.

In the second part of this chapter, we will introduce and discuss a stochastic framework for modeling of radio hardware impairments in terms of second-order statistics. Analytical expressions for the second order statistics is derived using the Bussgang theorem and the moment theorem for Gaussians. This approach is aimed toward applications in which oversampled time-domain signals are either not available or simply not useful, such as link- or system-level simulations. An example of numerical simulations for an OFDM-based massive MU-MIMO case is presented.

4.1 RF POWER AMPLIFIERS

Power amplifiers are known as the most nonlinear subsystem component of any radio transmitter. As such, modeling and understanding their behavior in order to compensate for the nonlinear distortion it produces in order not to violate the requirements set by the agreed upon standards is crucial.

3GPP defines two important metrics commonly used to quantify the linearity performance, which are error vector magnitude (EVM) and adjacent channel leakage ratio (ACLR). EVM specifically accounts for the performance between a base station (BS) and its scheduled users as it measured the in-band quality of the links. ACLR accounts for the interference leaked into the adjacent frequency channels which is crucial for the co-existence between networks to function. ACLR is a crucial metric for which the regulatory requirements are quite stringent in order to reduce the interference between networks and other applications in the same frequency band.

As power efficiency is highly important for reducing the environmental impact and the total cost of operation and the power amplifier being one of the major consumers of power, different efficiency enhancement technologies have been developed over the years. Amplifier topologies such as the Chireix [6] or the Doherty [8] amplifier, are commonly used, although the latter is more favored in recent scientific literature and in most industrial applications. This is in great measure due to its rather low implementation complexity compared to the Chireix amplifier and the performance in terms of power efficiency.

In more recent years, generalizations of the Doherty concept has been developed, supporting high efficiency over larger dynamic range. This further strengthens the Doherty amplifier in its position as the most popular amplifier topology. However, the improved efficiency performance comes at the cost of nonlinear behavior, [15], which may impact the overall system design depending on the transmit power.

The modeling needs vary in different applications and amplifier topologies, but in general the effects commonly covered in the literature are:

- Nonlinear transfer function and compression.
- Dispersive effects from impedance matching and bias networks.
- Electron traps from material artifacts.
- Long-term thermal memory effects due to heating and cooling.
- Load-modulation via mutual coupling in between antennas.

We will now briefly introduce the Volterra series and discuss some of the more common subsets of the Volterra series used in the scientific literature. Strengths and weaknesses of each model are also discussed and illustrated using measurements. Further on, we will discuss some of the more non-conventional models using orthogonal basis functions. We will end the section on power amplifier modeling with a discussion of global and local basis functions. It should be noted that the models discussed here are all acting in complex baseband and, thus, this carries no information regarding RF harmonics and other passband specific aspects.

4.1.1 THE VOLTERRA SERIES

The Volterra series dates back to 1887 [24] and may be considered as one of the most powerful tools for modeling not only radio power amplifiers, but nonlinear time invariant systems in general. The full Volterra series may be viewed as a superset of polynomial-based nonlinear models containing permutations of the input signal. As many of these are not always relevant in all modeling scenarios, many efforts have been made on pruning the full Volterra series in order to tailor it for specific amplifier topologies.

Much of the very early work on the Volterra series was performed over real-valued variables for passband systems. However, due to the quadrature nature of digital communication systems and the analytical manners by which these are modeled, the natural step of extending the Volterra series to complex variables was taken, [2].

The discrete-time, complex-valued Volterra series for causal systems with symmetric kernels ($\theta_{i,j} = \theta_{j,i}$) of nonlinear order P and memory-depth M can be written as

$$\begin{aligned} y[n] \;=\; & \sum_{p=1,3,5,\ldots}^{P} \sum_{m_1=0}^{M} \sum_{m_2=m_1}^{M} \cdots \sum_{m_{(p+1)/2}=m_{(p-1)/2}}^{M} \\ & \times \sum_{m_{(p+3)/3}=0}^{M} \cdots \sum_{m_p=m_{p-1}}^{M} \theta_{p,m_1,\ldots,m_p} \times \prod_{l=1}^{(p+1)/2} x[n-m_l] \prod_{j=(p+3)/2}^{p} \bar{x}[n-m_j]. \end{aligned} \tag{4.1}$$

We may note here that in the Volterra series, as stated in Eq. (4.1), there will always be an even number of conjugate terms accompanied by an odd amount of non-conjugate counterparts. This causes the frequent occurrence of terms in the form of $x[n-m_i]|x[n-m_j]|^p$, which plays an important role in power amplifier modeling, as the behavior is for a large part dependent on the signal envelope.

One beneficial aspect of any model based on the Volterra series is that they are linear in the parameters. This means that the model may be written as a simple matrix-vector multiplication,

$$\mathbf{y} = \mathbf{X}\boldsymbol{\theta}, \tag{4.2}$$

in which

$$\mathbf{X}(n,l) = \prod_{l=1}^{(p+1)/2} x[n-m_l] \prod_{j=(p+3)/2}^{p} \bar{x}[n-m_j] \tag{4.3}$$

is the nth row and lth column of the regression matrix and $\boldsymbol{\theta}$ is a vector containing the coefficients $\theta_{p,m_1,\ldots,m_p}$. This linear system of equations yields $\mathbf{y} = \big[y[0], \ldots, y[N]\big]^T$, which is the vector of output samples. Due to these models being parameter linear, the identification process is generally quite simple, provided that the regression matrix is numerically sound and not ill-conditioned.

The mean squared error (MSE)-optimal parameter estimate can be found as

$$\hat{\boldsymbol{\theta}} = \mathbf{X}^{+}\mathbf{y} \tag{4.4}$$

where we are making use of the Moore–Penrose pseudo-inverse, denoted $\mathbf{X}^{+}$.

4.1.2 COMMON SUBSETS OF THE VOLTERRA SERIES

The Volterra series as presented in Eq. (4.1) contains many terms which may not be providing useful degrees of freedom for accurate modeling. In order to avoid over- or noise-fitting by introducing unnecessary basis functions, some reductions of the Volterra series have been proposed over the years. We will now cover some of the more important ones.

4.1.2.1 Static Polynomial

The smallest and simplest subset of the Volterra series is that of the static polynomial. This model contains only terms at time n and can therefore not accurately model systems which are dispersive in nature. This excludes numerically accurate modeling of power amplifiers operating at a large fractional bandwidth, as these often exhibit dynamic memory effects, making the nonlinear behavior of the amplifier strongly frequency dependent. For narrow-band applications, however, the static polynomial model may very well be sufficient.

The static polynomial as it occurs in most literature is simply defined as

$$y[n] = \sum_{p=1}^{P} \theta_p x[n]|x[n]|^{2p-1} \tag{4.5}$$

where θ_p are the model parameters, sometime referred to as *kernels*. One very important observation regarding the static model, is that its asymmetries in the distortion spectrum may not be captured with this model as there is no memory involved. The output distortion spectrum will therefore always be symmetric around the center frequency.

Third-Order Static Polynomial

Most models covered in this chapter are aimed at accurate numerical predictive simulations or at providing a basis for DPD-algorithms. However, at certain points, simplified models may provide valuable insight in terms of analytical results. One special case of the static polynomial most suitable for this is that of the third-order static polynomial model. This is simply written as

$$y[n] = \theta_1 x[n] + \theta_2 x[n]|x[n]|^2. \tag{4.6}$$

Examples on how to use this model in conjunction with the moment theorem for Gaussians in order to analyze the impact of power amplifier distortion in massive MIMO arrays are shown in [18]. It may seem simplistic, but for amplifier operating in a reasonably nonlinear region, the third-order term is most commonly the more dominant one, even if higher-order terms are present. Thus, this may serve as a decent first-order approximation of a PA for analytical exercises, leading to valuable insight without having to struggle with tedious analytical manipulation.

4.1.2.2 A Note on Odd–Even and Odd Orders

Before moving on to more advanced behavioral models, we need to examine an issue which often occurs throughout the scientific literature. In regards to power amplifier behavioral modeling, there are mainly two different conventions used when defining the nonlinear orders of the model. These two conventions are commonly referred to as *odd–even-order* or just simply *odd-order* models. We will discuss this here using the static polynomial as an example, but the same reasoning applies for most Volterra-based models. The model which is written as

$$y[n] = \sum_{p=1}^{P} \theta_p x[n]|x[n]|^{2(p-1)} \tag{4.7}$$

is most commonly referred to as odd order, both since $2(p-1)$ is an odd number and since $x[n]|x[n]|^{2(p-1)}$ is a permutation of $x[n]$ an odd number of times. Another, slightly different convention commonly which is slightly less likely to occur in the scientific literature is written as

$$y[n] = \sum_{p=1}^{P} \theta_p x[n]|x[n]|^{p-1}, \tag{4.8}$$

in which the basis functions are referred to as odd–even, since the term $x[n]|x[n]|^{p-1}$ always is an odd permutation over $x[n]$, even if the power of $|x[n]|$ is allowed to be odd instead of solely even.

It has been claimed in the past that an odd–even model provides more degrees of freedom, [7], and should therefore provide a richer description of the amplifier behavior. However, this is a claim that has been rebuked by the authors of [13], who show that the odd–even- and odd-order models have the same modeling properties and the odd–even orders do not provide any richer description of the amplifier. This is a result of expanding the term $|x|$ in terms of $|x|^{2p}$, and showing that the series is uniformly convergent. The difference between orders in terms of modeling accuracy is in fact proportionality to the model truncation error.

Moving on, we will in this chapter stick to the more common odd-order version in the following sections as this is the conventional ordering in most publications.

4.1.2.3 Memory Polynomial

The first natural extension of the static polynomial is to add memory terms in order to model dispersive effects introducing a frequency selective behavior. The memory polynomial (MP) model as described in [12], can be written in its complex baseband form as

$$y[n] = \sum_{p=1}^{P} \sum_{m=1}^{M} \theta_{p,m} x[n-m]|x[n-m]|^{2(p-1)}, \tag{4.9}$$

where P is the nonlinear order and M is the memory depth. From Eq. (4.9), we see that the MP is in principle a nonlinear finite impulse response (FIR) filter. As described in [20], the MP is an extension to the common Hammerstein model in which a nonlinear function is followed by a linear filter.

In the MP model only diagonal memory terms from the Volterra series are included, which in some cases may limit the modeling capabilities, particularly in the case that the amplifier in question displays a strong, nonlinear memory for which cross-terms will be necessary. For simpler applications and for analytical manipulation, this model is often good enough and easy to use.

4.1.2.4 Generalized Memory Polynomial

The generalized memory polynomial (GMP) was first presented in [20]. GMP extends the aforementioned MP by introducing cross-terms in the memory-domain [12], which is written as

$$\begin{aligned} y[n] &= \sum_{p=1}^{P} \sum_{m=1}^{M} \alpha_{p,m} x[n-m]|x[n-m]|^{2(p-1)} \\ &+ \sum_{p=1}^{P} \sum_{m=1}^{M} \sum_{l=1}^{L} \beta_{p,m,l} x[n-m]|x[n-m-l]|^{2(p-1)} \\ &+ \sum_{p=1}^{P} \sum_{m=1}^{M} \sum_{l=1}^{L} \gamma_{p,m,l} x[n-m]|x[n-m+l]|^{2(p-1)} \end{aligned} \tag{4.10}$$

where P is the nonlinear order, M is the memory depth and L is the number of leading and lagging cross-terms. In this model, the memory terms span an L-dimensional strip in the memory-space of the Volterra series. Reference [20] also introduces a more general way of creating the model using index arrays in order to facilitate pruning of the parameter space in order to achieve the desired complexity/performance trade-off.

4.1.3 GLOBAL VS. LOCAL BASIS FUNCTIONS

All of the models examined so far are using so-called global basis functions. This is in the sense of basis functions acting upon the entire range of the envelope. This may in some cases cause numerical issues, in particular when using high-order polynomial basis functions in conjunction with signals, which has a large dynamic range combined with low probabilities of occurring peaks. This will end up causing a poor numerical fit as the number of samples collected around the peak power will be small, which tends to have a negative impact particularly on the high-order terms as their estimator variance rapidly increases with order.

One straightforward solution to this numerical issue is to use so-called local basis functions. By this, we mean dividing the envelope-space into segments which then get associated with their own specific set of basis functions. Let $\mathcal{P}$ be the envelope-range which we divide into Ω-ordered sections as

$$\mathcal{P} = \bigcup_{\omega=1}^{\Omega} \mathcal{P}_u \tag{4.11}$$

where $\mathcal{P}_u \cap \mathcal{P}_{u'} = \varnothing$ for $u \neq u'$. We can now use this to form modified versions of the models previously discussed. For example, examining the static polynomial, we can write

$$y[n] = \sum_{p=1}^{P} \sum_{\omega=1}^{\Omega} \mathbf{I}_{|x[n]| \in \mathcal{P}_\omega} \theta_p x[n] |x[n]|^{2(p-1)}, \tag{4.12}$$

in which $\mathbf{I}$ is the indicator function. It may be difficult to see from the equation above, but this yields a regression matrix which is largely sparse, e.g. the majority of elements will be zero. This may increase the overall numerical complexity of the model, but as the regression matrix will have a sparse structure, this complexity may be reduced using sparse matrix methods for computation.

In Fig. 4.1, we see one example of a static polynomial fitted with local basis functions on data generated via a memoryless polynomial. As the number of sections increases, we increase the modeling accuracy at the cost of added complexity.

Quite simple examples of local basis functions may be in the form of a look-up table (LUT) in which elements of the table only act upon its own specific region of the envelope. Another example which allows for switching between local cross-terms in the memory-space, is the so-called vector-switching model [1].

4.1.4 EXPERIMENTAL MODEL VALIDATION

Concluding the discussion on power amplifier modeling, the numerical accuracy will be examined using a set of measurements performed on a Gallium-Nitride (GaN)-based class-AB amplifier using the web-lab system have been used [14]. The models considered in this chapter will be the static polynomial, the GMP, and a vector-switching extension of the GMP. For easy quantification of the model performance, we need a set of metrics.

4.1.4.1 Quantifying Modeling Performance

In order to make a sound selection of the model to suit the application in mind, we need to examine how these behave using measurement data. For this purpose, we need to consider a couple of important figures of merit. One of the most commonly used figures of merit is the normalized mean squared error (NMSE). Here, we compare the measured and modeled output over the entire measurement bandwidth. The modeling error is then normalized with the measured output variance in order to make the figure

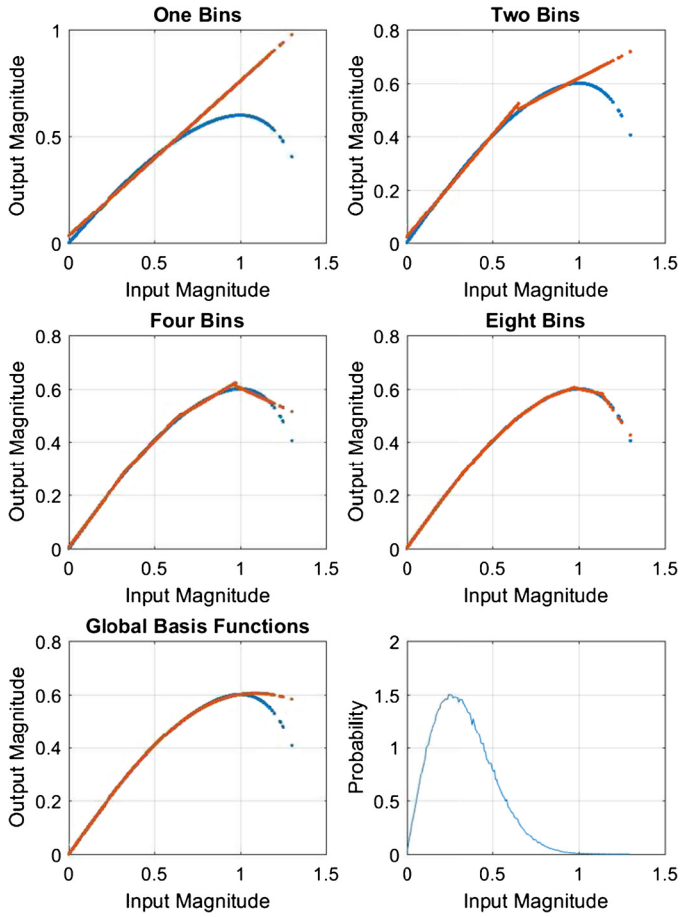

FIGURE 4.1

Illustration of local vs. global basis functions. An illustration of how local basis functions fit to a static model reference. Here, piecewise linear functions are used over different numbers of envelope bins.

power independent. NMSE is commonly defined as

$$\text{NMSE} = \frac{\sum_{n=0}^{N} |y_{\text{meas}}[n] - y_{\text{mod}}[n]|^2}{\sum_{n=0}^{N} |y_{\text{meas}}[n]|^2} \tag{4.13}$$

Table 4.1 Model validation results

PA model	NMSE (dB)	ACEPR (dB)
Static polynomial	−28.5	−29.0
GMP	−32.5	−33.5
VS-GMP	−37.0	−38.0

where y_{meas} is the measured output and y_{mod} is the modeled output. Compared to conventional MSE, the NMSE removes any power dependencies, enabling comparison over different power ranges if necessary.

The second figure of merit useful to assess the modeling performance is the adjacent channel error power ratio (ACEPR), which provides a measure of how accurate the model predicts the generated adjacent channel distortion. The ACEPR is defined as

$$\text{ACEPR} = \frac{\int\limits_{\text{Adj. band}} |y_{\text{meas}}(f) - y_{\text{mod}}(f)|^2 \, df}{\int\limits_{\text{Adj. band}} |y_{\text{meas}}(f)|^2 \, df}. \tag{4.14}$$

We may in ACEPR observe similarities to NMSE, but with the emphasis put on modeling of the distortion outside of the assigned channel.

In order to evaluate the modeling performance, we need two sets of measurement data—one for identification and one for evaluation. This is required to provide a fair comparison such that the model is not fitted to one specific signal realization. In this experiment, we use filtered complex Gaussian noise which commonly has statistical properties very similar to any wide-band OFDM-based system due to the central limit theorem. Since we are not evaluating a postdecoding metric such as bit error rate (BER), Gaussian noise is sufficient.

Fig. 4.2 depicts the measured power spectral density (PSD) and amplitude-to-amplitude modulation (AMAM) of the identification and evaluation data in terms of instantaneous normalized gain.

The model parameters are then found using the Moore–Penrose pseudo-inverse as described in Eqs. (4.3) and (4.4). After performing the identification, each model runs with the evaluation data which is compared to the measurements. The results in terms of NMSE and ACEPR are presented in Table 4.1.

In order to further illustrate the modeling capacities for each case, we may examine the AMAM characteristics and PSD from measurement data. Fig. 4.3 illustrates the measured and simulated AMAM. Fig. 4.4 shows the corresponding simulated PSD for the models.

As we may observe, the static polynomial shows no dispersion effects due to its inherent lack of memory. The GMP however, is capable of modeling these effects as shown. As this particular amplifier is quite nonlinear, Fig. 4.3 illustrates the manner in which with both the static polynomial and the GMP with global basis functions are having certain difficulties fitting to the data near peak power. This is however not the case for the VS-GMP, which further improves the modeling accuracy by applying local basis functions. In each region of the envelope, a low-order GMP ($P = 3$) is applied. Further

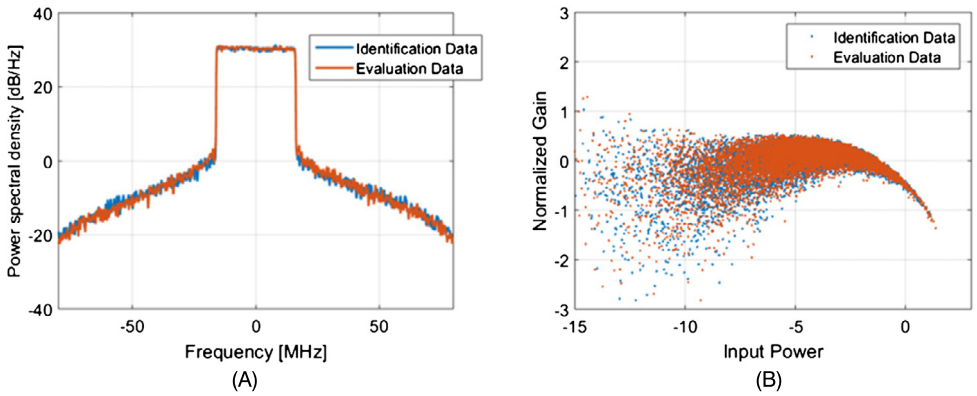

FIGURE 4.2

Measured PSD (A) and AMAM (B) characteristics of the identification and evaluation data used in the comparison between models.

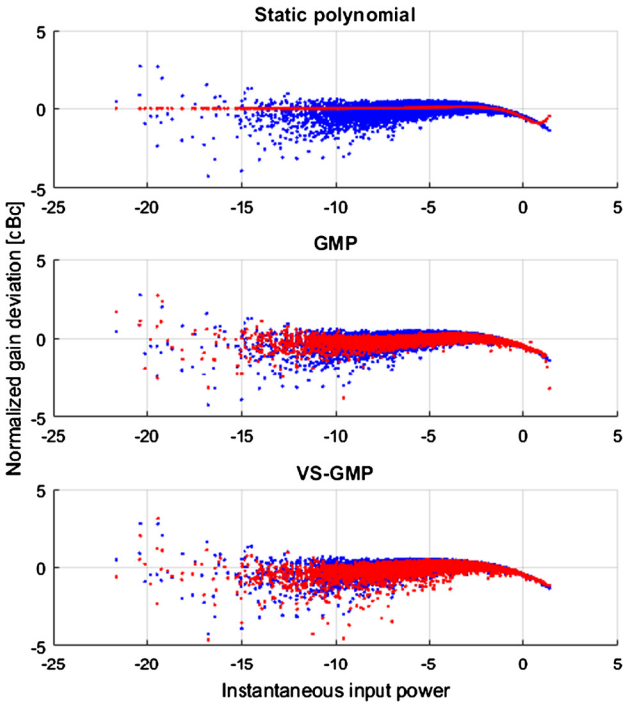

FIGURE 4.3

Comparison between measurement and models. Comparative simulations between the static polynomial model and the GMP, both with global and local basis functions. Blue (dark gray in print version) curves denote measurement data, red (light gray in print version) curves denote predicted output from the models.

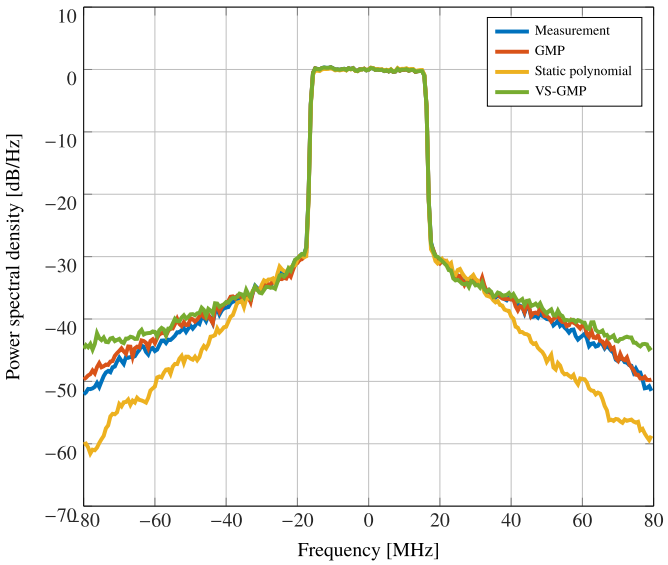

FIGURE 4.4

Comparative simulations between the static polynomial model and the GMP using global and local basis functions.

practical comparisons between models using global and local basis functions may be found in [1]. The numerical results are summarized in Table 4.1.

4.1.5 MUTUALLY ORTHOGONAL BASIS FUNCTIONS

A less common, yet useful model for power amplifier modeling is constructed by using mutually orthogonal basis functions. Consider the expansion of a nonlinear function using the basis functions H_p,

$$y[n] = \sum_{p=1}^{P} \theta_p H_p(x[n]). \tag{4.15}$$

These basis functions can be designed to be mutually orthogonal with respect to the statistics of our input signal. That implies, for all p, k, that the property

$$\mathbb{E}\left[H_p(x[n])H_k^*(x[n])\right] = 0 \tag{4.16}$$

needs to hold. For the case of a complex Gaussian distributed input signal, we can achieve this mutual orthogonality by using the complex Itô-generalization of the Hermitian polynomials, at least for a given input power σ_x^2.

The mutual orthogonality between each basis function may also be beneficial as it provides a description in which the linear term, e.g. the useful signal part, is orthogonal to the distortion as this is a

linear combination of the remaining, mutually orthogonal components. We write this as

$$y[n] = s[n] + d[n] \tag{4.17}$$

where

$$s[n] = \theta_1 H_1(x[n]) \tag{4.18}$$

is the linearly scaled input signal and

$$d[n] = \sum_{p=2}^{P} \theta_p H_p(x[n]) \tag{4.19}$$

is the distortion which is expressed using the complex Itô polynomials; now these are mutually orthogonal to the input signal,

$$\mathbb{E}[s[n]d^*[n]] = 0. \tag{4.20}$$

The property of mutual orthogonality provides a clearer path to determining the statistical properties of the distortion in terms of its covariance matrix, in a similar manner as the linear stochastic model discussed in Chapter 4.4.

This approach provides a simple way of analyzing of the spatial properties of the distortion, in the context of MU-MIMO [17]. Here, it is shown that

$$\frac{K^3 + K^2}{2} L^2 v(f) \tag{4.21}$$

where K is the number of users or transmit-directions, L is the number of significant taps of the channel and $v(f)$ is a constant depending on the excess bandwidth. A necessary condition for the distortion to behave omni-directionally is

$$\frac{K^3 + K^2}{2} L^2 v(f) \geq M. \tag{4.22}$$

As Fig. 4.5 illustrates, we see that, as the number of users increases from $K = 1$ to $K = 3$ and 10, the number of dominant directions increases with $\frac{K^3+K^2}{2}$ (as this is modeled using a frequency-flat, narrow-band channel with $L^2 v(f) = 1$). A few further observations may be made from Fig. 4.5 is that the radiated adjacent power is at worst in parity with the single-antenna case. This occurs only in the case of $K = 1$ and only towards the user served. Everywhere else, any potential victim user will receive less distortion compared to the corresponding single-antenna case.

As K then increases, the adjacent channel power is divided over more directions than that of the in-band signal. Thus, it never reaches the same radiated power as in the single-antenna case. This indicates that, in most practical cases, the impact of the radiated distortion will be less in a large array than in the case of a single-antenna system. More discussion and rigorous derivation of the radiation patterns can be found in [17].

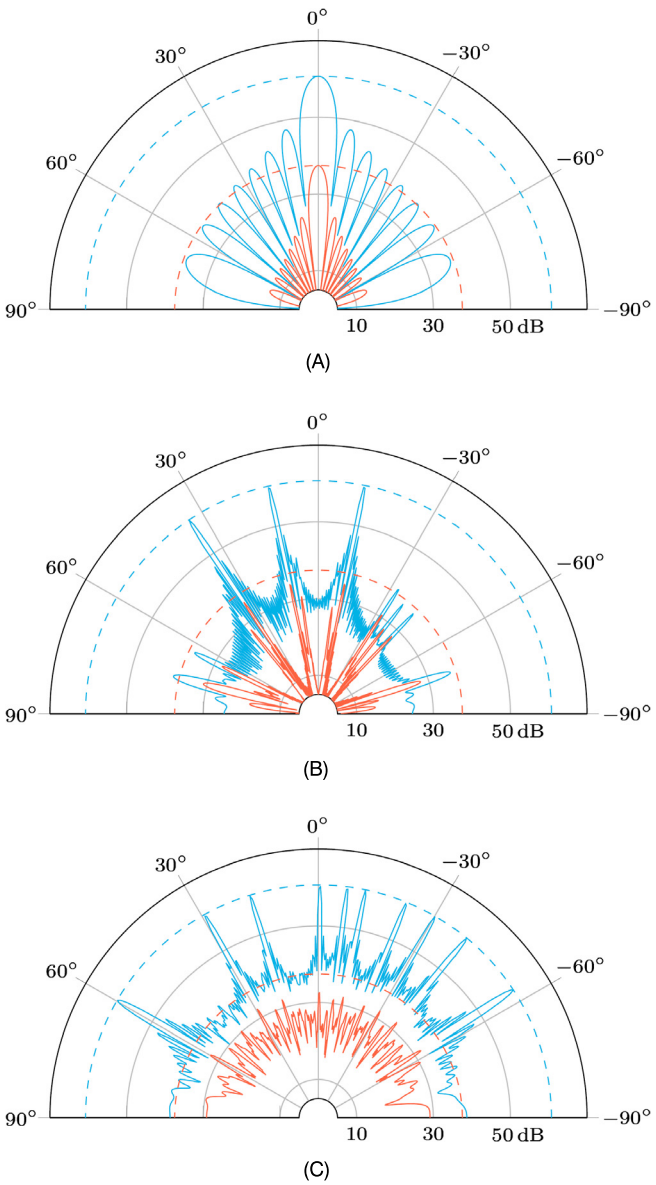

FIGURE 4.5

Radiation patterns from uniform linear arrays. Blue (dark gray in print version) curves indicate the in-band radiated power. Red (light gray in print version) curves indicate the power radiated in the adjacent channel. The dashed lines correspond to the single-antenna case with the same ACLR. (A) Radiated pattern for in- and adjacent-band in the case of $K = 1$ and $M = 16$, (B) radiated pattern for in- and adjacent-band in the case of $K = 3$ and $M = 128$, (C) radiated pattern for in- and adjacent-band in the case of $K = 10$ and $M = 128$.

4.1.6 MULTI-ANTENNA ENVIRONMENTS AND MUTUAL COUPLING

Another aspect of power amplifier modeling which has become increasingly important in multiantenna applications is modeling of the mutual coupling between the antennas and its impact on the power amplifier behavior. This coupling can create a signal-dependent and time-varying load-impedance seen by the amplifier, which in turn changes the behavior in terms of the instantaneous transducer gain. Such effects may be seen by plotting the normalized instantaneous gain, as shown in Fig. 4.7. The large variation of instantaneous gain, which may be seen in Fig. 4.7, is caused by load-modulation of the power amplifier via mutual coupling between branches.

In order to model the effects of mutual coupling, we need to view the power amplifier as a dual-input system in which the second added input is the reflected wave stemming from the transmitted signals from neighboring transmitters, transfered via mutual coupling between antennas as illustrated in Fig. 4.6. Here, $x_1, \ldots, x_M$ are the M transmit signals and $y_1, \ldots, y_M$ the M output signals affected by the nonlinear distortion of the power amplifiers. We also need the variables $y_{r,1}, \ldots, y_{r,M}$, which are mixtures of transmit signals being reflected back into each amplifier via the coupling.

At every time instant n, we may compute the reflected wave to the antenna port m as the scalar product

$$y_{r,m} = \mathbf{y}^T \boldsymbol{\lambda}_m, \tag{4.23}$$

in which $\boldsymbol{\lambda}_m = [\lambda_m 1m, \ldots, \lambda_{Mm}]$ is the parameter vector describing the mutual coupling and $\mathbf{y} = \left[y_1, \ldots, y_M\right]$ is the vector of the transmitted signals.

The first approach to modeling such effects was proposed by Root et al. [22], through a model referred to as the polyharmonic distortion (PHD) model. As a large-signal extension to the S-parameters, and thus nonlinear, this model is, however, quasistatic in nature. This has led to the development of an extension based on the memory polynomial, as derived and validated in [9]. We have

$$\begin{aligned} y_m[n] &= \sum_{p=1}^{P}\sum_{m=1}^{M_1} \alpha_{p,m} x_m[n-m_1]|x_m[n-m_1]|^{2p-1} \\ &+ \sum_{p=1}^{P}\sum_{m_1=1}^{M_1}\sum_{m_2=1}^{M_2} \beta_{p,m,l} y_{r,m}[n-m_2]|x_m[n-m_1]|^{2p-1} \\ &+ \sum_{p=1}^{P}\sum_{m_1=1}^{M_1}\sum_{m_2=1}^{M_2} \gamma_{p,m,l} x_m^2[n-m_1] y_{r,m}^*[n-m_2]|x_m[n-m_2]|. \end{aligned} \tag{4.24}$$

It shares some features with the model in [22], namely the occurrence of the conjugate terms in the reflected wave ($y_{r,m}^*$). The conjugate term occurs due to non-analyticity of the describing function. This goes against conventional Volterra theory in which the number of conjugates in each basis function is always even and accompanied by an uneven and larger number of non-conjugated terms, forming basis functions in the form $x[n]|x[n]|^p$.

The model stated in Eq. (4.24) is parameter linear in the time domain and is suitable for wide-band applications as it supports memory in both incident and reflected waves. As memory is included also in the reflected term, the description of the crosstalk network stated in Eq. (4.23) is no longer sufficient. The modification is, however, rather small as the coupling coefficients $\boldsymbol{\lambda}$ are linear and may be modeled by conventional FIR-filters.

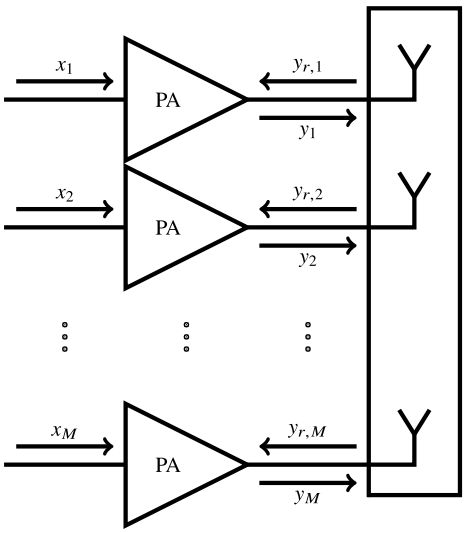

FIGURE 4.6

System model for the dual-input model. The system model for an active antenna system with nonlinear amplifiers. The reflected signal caused by mutual coupling causes a time-varying behavior which is not captured by conventional models.

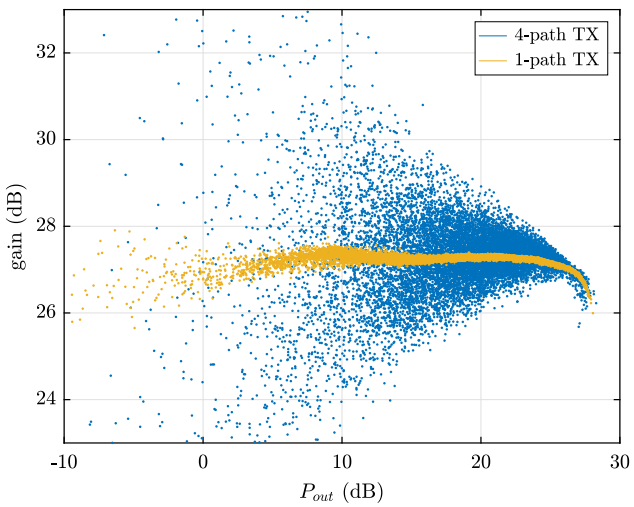

FIGURE 4.7

Measured instantaneous gain. Normalized instantaneous gain of a power amplifier with (blue; dark gray in print version) and without (yellow; light gray in print version) the impact of mutual coupling.

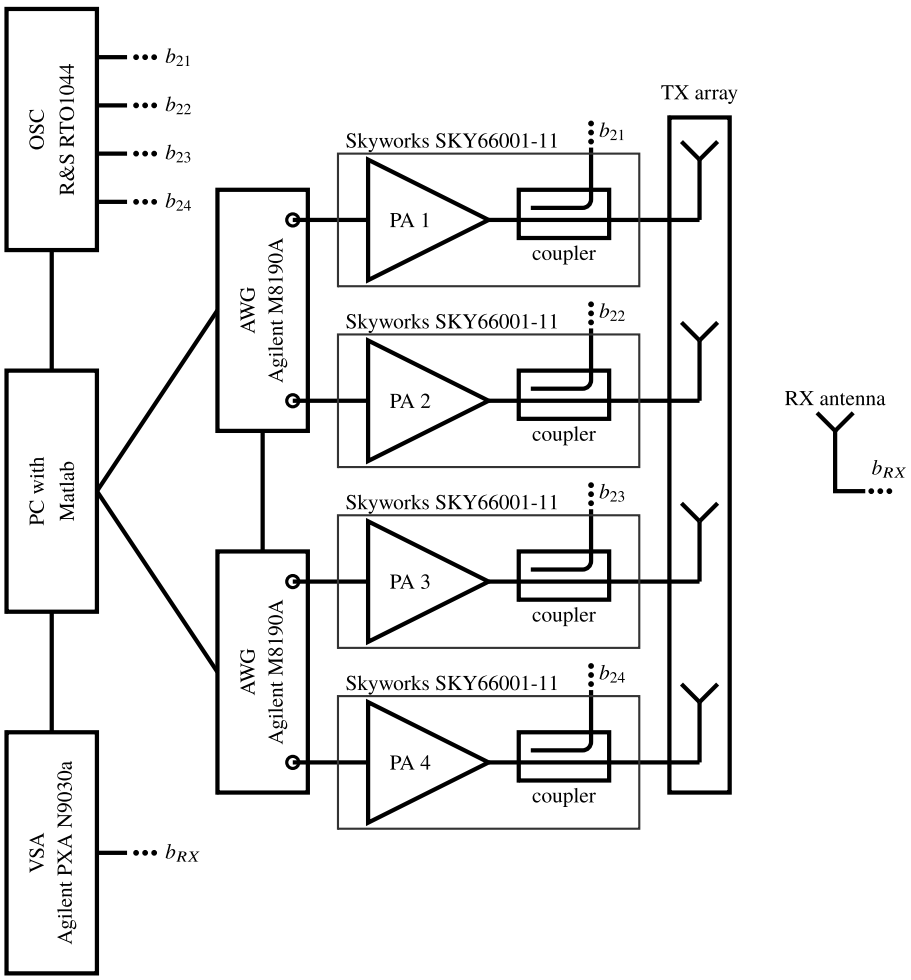

FIGURE 4.8

Measurement setup for model validation. The system model for an active antenna system with nonlinear amplifiers. The reflected signal caused by mutual coupling causes a time-varying behavior which is not captured by conventional models.

The model described in Eq. (4.24) is validated via measurements presented in [9]. These measurements were performed both conducted at the amplifier output reference plane, as well as over the air using a reference receiver. Using wide-band arbitrary waveform generators as shown in Fig. 4.8, four power amplifier modules were connected to two different configurations of a 2×2 patch antenna. The measured characteristics of these arrays are shown in Fig. 4.9. As shown, the two arrays have, via variations in patch separation, different amounts of coupling. The spectrum plots shown in Fig. 4.9 are for the case of strong mutual coupling.

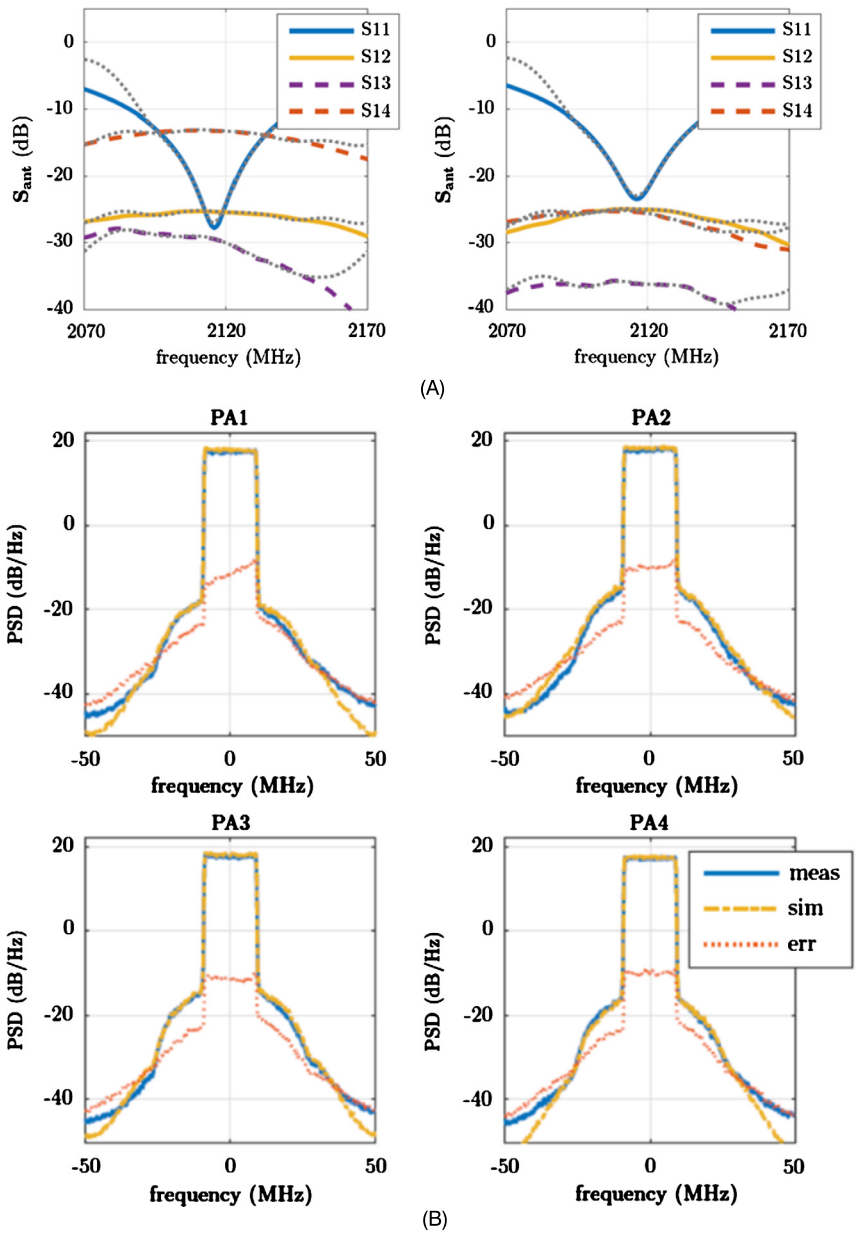

FIGURE 4.9

Antenna array characteristics and measured power spectral density (A) Measured S-parameter characteristics of the two different 2x2 patch-antenna arrays used in the validation process. To the left, the antenna spacing is 0.5λ and to the right 0.7λ, (B) measured and simulated output power spectrum from each of the four power amplifiers, followed by the model error spectrum.

4.2 OSCILLATOR PHASE NOISE

Local oscillators are the main source of phase noise in radio communication systems. It mainly stems from imperfections in both the passive and active parts of the oscillator circuitry, which in turn inflicts several types of noise sources. Some of these imperfections are:

- Thermal noise.
- Flicker or $1/f$ noise.
- Shot noise.
- Finite Q-value of resonator tank.

Together, this forms what we refer to as phase noise.

The impact of most of these sources may be mitigated by different means, for example using a PLL or simply increasing the current pumped into the resonator tank. There are drawbacks to each of these methods such as increased power consumption or increment of other noise in other parts of the spectrum. And with the trend of phase noise rapidly increasing with frequency, it is of utter importance that these effects are accurately modeled and studied. In particular, analysis of phase noise and its impact on OFDM has been performed to a very large extent.

4.2.1 PHASE-NOISE POWER SPECTRUM AND LEESON'S EQUATION

One of the early studies on phase noise conducted by Leeson in 1966, resulted in an empirical expression for phase-noise power spectral density which is commonly used to this day [16]. The power spectrum approximation is often described by

$$L(f_m) = 10\log_{10}\left[\frac{1}{2}\left(\left(\frac{f_0}{2Q_l f_m}\right)^2 + 1\right)\left(\frac{f_c}{f_m} + 1\right)\left(\frac{FkT}{P_s}\right)\right], \tag{4.25}$$

in which some relevant circuit factors are used as parameters. Here, f_0 is the operating frequency of the oscillator, Q is the loaded Q-value of the oscillator, f_m is the offset frequency at which we observe the phase noise, f_c is the $1/f$ cutoff frequency, F is the noise figure of the buffer amplifier, k is Boltzmann's constant, T is the temperature in Kelvin, and P_s is the output power of the oscillator.

Examining the power spectral density as illustrated in Fig. 4.10, the overall phase noise increases with roughly 6 dB per doubling of the center frequency. Although Leeson's equation is an empirical model, it has stood the test of time and is still commonly cited and used to predict phase-noise performance or to trade phase noise for power consumption. We will now discuss an approach used for simplistic modeling of phase noise in the presence of a phase-noise tracker.

4.2.2 PHASE-NOISE MODELING: FREE-RUNNING OSCILLATOR

As it is common to describe a communication system in discrete time due to the nature of its digital implementation, we will stay with phase-noise modeling in the discrete-time domain here. The scientific literature is however not limited to discrete time modeling as a Wiener-process may be formed in continuous time as well.

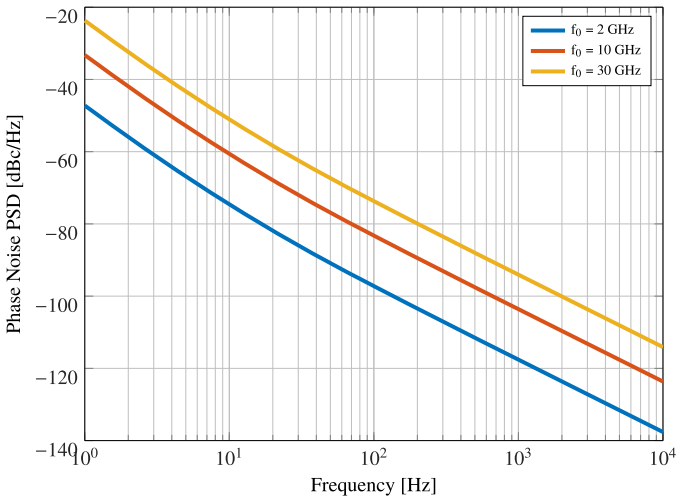

FIGURE 4.10

Phase-noise power spectral density. Phase-noise power spectral density according to Leeson's approximation for different center frequencies, $f_0 = 2$, 10, and 30 GHz.

Phase noise is multiplicative in its nature and applied as

$$y[n] = x[n]e^{i\varphi[n]}, \tag{4.26}$$

in which the phase-noise component φ is commonly modeled using a random walk process,

$$\varphi[n] = \varphi[n-1] + w[n]. \tag{4.27}$$

Just as in the continuous time case, this is an accumulative process in which the variance of φ grows over time. In the presence of a phase-noise tracker, either in the shape of a phase-locked loop or a tracker at the receiver, we may model the residual phase noise as an autoregressive process,

$$\varphi[n] = \lambda\varphi[n-1] + w[n]. \tag{4.28}$$

Here, $w \sim \mathcal{N}(0, \sigma_w^2)$ is the innovation noise and $0 < \lambda < 1$ is a constant determined mainly by the PLL. This phase-noise model is a wide-sense stationary (WSS) process which has the autocorrelation function

$$\mathbb{E}\{\varphi[n]\varphi[n-l]\} = \begin{cases} \dfrac{4\pi^2 f_c^2 t_s \kappa \lambda^{|l|}}{1-\lambda^2} & \text{if } m = m', \\ 0 & \text{else,} \end{cases} \tag{4.29}$$

where f_c is the center frequency, t_s is the sample-time, and κ is a constant depending on the quality of the oscillator and $\varphi \sim \mathcal{N}(0, 4\pi^2 f_c^2 t_s \kappa)$. Examples of the simulated power spectral density for three

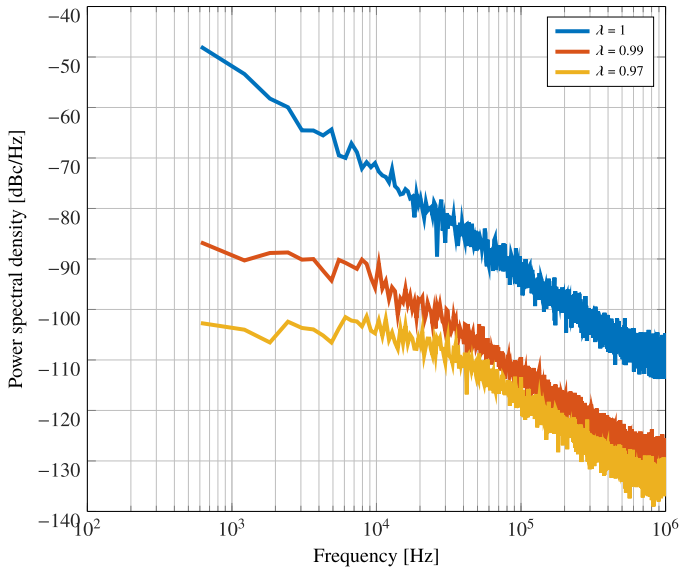

FIGURE 4.11

Phase-noise power spectral density. Simulated phase-noise spectral density using the model in (4.26)–(4.28) with three different values of λ.

different values of λ are shown in Fig. 4.11. Notice the flattening of the spectrum near the carrier frequency as λ decreases.

In practical applications, decreasing λ is analog to increasing the PLL-bandwidth which improves the phase noise around the carrier. However, this tends to increase the white noise part at higher offset frequencies, something which is not captured by this particular model.

4.2.3 PHASE-NOISE MODELING: PHASE-LOCKED LOOP

The phase noise of the PLL-based oscillator consists of three main noise sources, i.e., noises from the reference oscillator θ_{ref}, the phase–frequency detector and the loop filter θ_{LP}, and the voltage controlled oscillator (VCO) θ_{VCO}, as shown in Fig. 4.12. The Laplace transform of the phase noise of the PLL-based oscillator is given as [26]

$$\theta_{\text{out}} = \frac{N_{\text{D}} K_{\text{VCO}} Z(s) \left(K_{\text{D}} \theta_{\text{ref}} + \theta_{\text{LP}}\right) + s N_{\text{D}} \theta_{\text{VCO}}}{s N_{\text{D}} + K_{\text{D}} K_{\text{VCO}} Z(s)}, \tag{4.30}$$

where K_{D} denotes the gain of the phase–frequency detector, K_{VCO} represents the sensitivity of the VCO, $Z(s)$ represents the loop filter, and $1/N_{\text{D}}$ is the frequency divider. The noise sources include both white noise (thermal noise) and colored noise (flicker noise). The PSD of the noise source can be

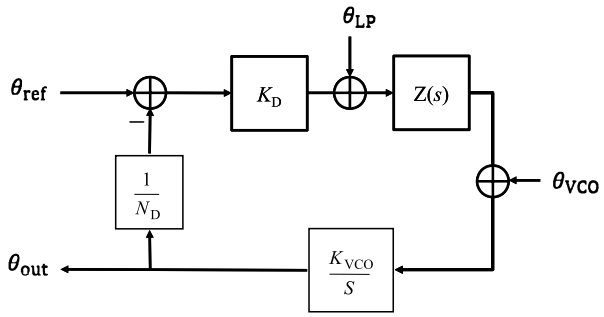

FIGURE 4.12

Phase-noise model of PLL-based oscillator. Blockdiagram of the phase-noise model for a PLL-based oscillator.

modeled as [26]

$$S(f) = S_0 \frac{1+\left(\frac{f}{f_z}\right)^2}{1+\left(\frac{f}{f_p}\right)^2} + S_0 \frac{1+\left(\frac{f_{zo}}{f_z}\right)^2}{1+\left(\frac{f_{zo}}{f_p}\right)^2}\left(1+\left(\frac{f_{zo}}{f_{po}}\right)^k\right)\frac{1}{1+\left(\frac{f}{f_{po}}\right)^k}, \tag{4.31}$$

where S_0 is the power density at zero frequency, f_p and f_z are the (3-dB) pole and corner frequencies of the thermal noise, respectively, $k = 1$ and 3 for flick noises of the PLL and of the oscillator, respectively, and f_{po} and f_{zo} are the pole and corner frequencies of the flicker noise, respectively. The detailed modeling parameters are listed in Table 4-2 of [26]. As an example, Fig. 4.13 shows the estimated PSDs of the carrier phase noise at 6, 28 and 60 GHz, respectively.

4.3 DATA CONVERTERS

Data converters are known as bottlenecks in digital communication systems as the transceiver bandwidths increases, while at the same time demands on dynamic range increase via denser modulation schemes. Amongst the sources of impairment related to data converters, the one most commonly modeled is the quantization noise. As data converters are mixed-signal components, issues with nonlinearities caused by either un-even quantization levels or output buffer amplifiers have also been modeled in the past, quite often using a Volterra series approach [4].

4.3.1 MODELING OF QUANTIZATION NOISE

The modeling of quantization noise is an area well mapped out and the study on quantization is therefore a quite mature field. Some of the most important foundations can be found in [25,23]. Part of this has led to a commonly used simplification of modeling a quantizer by adding uniform noise:

$$\mathcal{Q}(x) = x + w \tag{4.32}$$

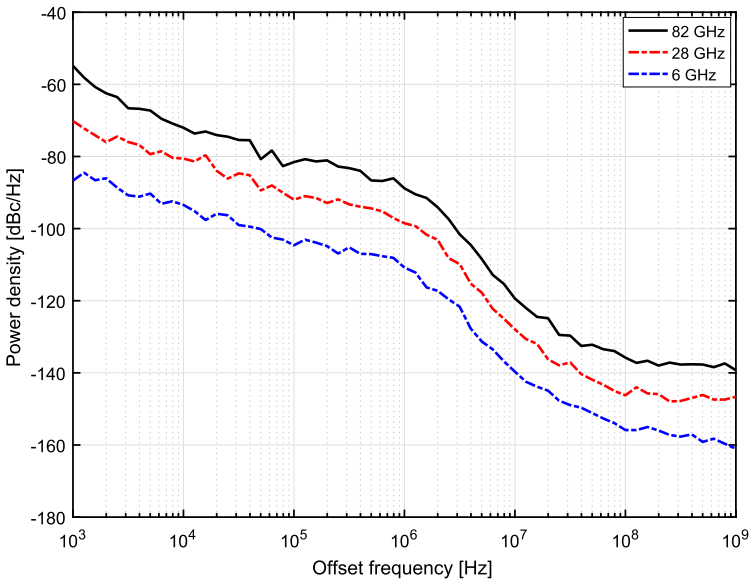

FIGURE 4.13

The PSD of the carrier phase noise. Simulated PSD of the phase noise generated by the model in Fig. 4.12, parameterized for three different center frequencies.

where $\mathcal{Q}$ denotes the quantizer function and w is an additive noise process with parameters determined by the quantizer properties and the input signal statistics. Under certain constraints, the signal to quantization noise ratio (SQNR) is modeled as

$$\text{SQNR} \approx 6.02q \tag{4.33}$$

where q is the number of bits used. This is, however, not always a good approximation depending on the input signal statistics. More exact conditions for when the quantization noise is uniform have been presented in [23]. For the general case using a DAC or ADC with q bits, we have a discrete set of 2^q possible outputs from the quantizer. Most commonly, uniform mid-rise quantizers are assumed; however, other alternatives exist. Given a finite range of the possible input signal, the quantizer can be modeled as

$$\mathcal{Q}(x) = \begin{cases} \frac{\Delta}{2}(1-2^q) & \text{if } x < -\frac{\Delta}{2}2^q, \\ \Delta\lfloor\frac{x}{\Delta}\rfloor + \frac{\Delta}{2} & \text{if } |x| < \frac{\Delta}{2}2^q, \\ \frac{\Delta}{2}(2^q-1) & \text{if } x > \frac{\Delta}{2}2^q, \end{cases} \tag{4.34}$$

in which Δ denotes the LSB size. For a quadrature signal, represented by a complex random variable, we define the input–output relation for the set of baseband DAC's or ADC's by

$$f_{\text{DAC}}(x) = \mathcal{Q}(\text{Re}x + i\,\text{Im}x) = \mathcal{Q}(\text{Re}x) + i\,\mathcal{Q}(\text{Im}x)\,. \tag{4.35}$$

As exact modeling of the quantization noise may be difficult and linear, stochastic approaches as proposed in [10] may be sufficient, but we will leave the discussion for Section 4.7.

4.4 STATISTICAL MODELING

In certain applications such as system-level performance assessment, it may be difficult to make use of behavioral models as they often operate on oversampled time-domain signals. In most communication system engineering applications, the signals are modeled as stochastic random variables with given second-order statistics described with a covariance matrix. As such a signal passes through a nonlinear function, for example a building block, the statistical properties changes. With advanced multiantenna systems making use of the spatial properties of the communication channel, the importance of knowing the second-order statistics increases as it determines the spatial properties of both the transmit signal as well as the hardware impairments.

4.4.1 THE BUSSGANG THEOREM AND THE SYSTEM MODEL

Determining the second-order statistics of the distortion is straightforward using the Bussgang theorem. Let $f(\cdot)$ be a nonlinear function and $x \sim \mathcal{N}(0, \sigma_x^2)$. The input–output cross-covariance is equal to the input autocorrelation up to a constant C [5], as

$$R_{f(x),x} = C R_x. \tag{4.36}$$

This property may be used in order to formulate a linear stochastic model which describes the output of a nonlinear system when the input is modeled using a Gaussian random variable x. The model is written as

$$f(x) = \alpha x + d \tag{4.37}$$

where $d \sim \mathcal{N}(0, \sigma_d^2)$ is the distortion noise which is orthogonal to the scaled input signal αx and α is the gain constant, determined by

$$\alpha = \frac{\mathbb{E}\left[x \bar{y}\right]}{\sigma_x^2}. \tag{4.38}$$

From this, we have $\mathbb{E}\left[\alpha x \bar{d}\right] = 0$. For the multiantenna case, considering a system with M antennas, we may model this in matrix-vector format as

$$\mathbf{y} \quad = \quad \mathbf{G}\mathbf{x} + \mathbf{e} \tag{4.39}$$

where $\mathbf{G}$ is the complex gain matrix and $\mathbf{e}$ is the distortion noise. The gain matrix is defined as

$$\mathbf{G} = \text{diag}\left(\mathbb{E}\left[x_1 \bar{y}_1\right], \ldots, \mathbb{E}\left[x_M \bar{y}_M\right]\right). \tag{4.40}$$

The remaining distortion noise, which is orthogonal to $\mathbf{Gx}$, is then distributed as

$$\mathbf{e} \sim \mathbb{C}\mathcal{N}\left(\mathbf{0}, \mathbf{C_e}\right) \tag{4.41}$$

where

$$\mathbf{C_e} = \mathbf{C_y} - \mathbf{G}\mathbf{C_x}\mathbf{G}^H, \tag{4.42}$$

which forces $\mathbf{e}$ and $\mathbf{x}_n$ to be mutually orthogonal. This description is equivalent to the model discussed in Section 4.1.5 as they have exactly the same properties, which stems from using mutually orthogonal basis functions in the shape of Itô–Hermite polynomials.

4.5 STOCHASTIC MODELING OF POWER AMPLIFIERS

In the case of power amplifiers, derivation of the distortion covariance is straightforward by repeatedly using the moment theorem for Gaussians [21]. This may, however, be tedious, as the number of cross-products and higher-order moments tends to explode. For this reason, we will stick to the canonical third-order model here. Using the common third-order polynomial as foundation, written as

$$y[n] = \theta_1 x[n] + \theta_2 x[n]|x[n]|^2, \tag{4.43}$$

we would, as illustrated in [10], be able to derive the model in the following form:

$$\mathbf{y} \quad = \quad \mathbf{G}^{\text{PA}}\mathbf{x} + \mathbf{e}^{\text{PA}}. \tag{4.44}$$

Here $\mathbf{G}^{\text{PA}} = \mathbf{I}_{MN} \otimes \text{diag}\left(\mathbf{g}^{\text{PA}}\right) \in \mathbb{C}^{MN \times MN}$, or more explicitly

$$\mathbf{G}^{\text{PA}} = \mathbf{I}_{MN} \otimes \left(\theta_1 \mathbf{I}_{MN} + 2\theta_2 \text{diag}(\mathbf{C_x})\right). \tag{4.45}$$

The distortion covariance due to orthogonality will become

$$\mathbf{C}_{\mathbf{e}^{\text{PA}}} = \mathbf{C_y} - \mathbf{G}^{\text{PA}}\mathbf{C_x}(\mathbf{G}^{\text{PA}})^H \tag{4.46}$$

in which $\mathbf{G}^{\text{PA}}$ is given by Eq. (4.45), $\mathbf{C_x}$ is the transmit covariance matrix which is given by precoder design and $\mathbf{C_y}$ is the covariance matrix of the distorted output. This has to be manually computed using the moment theorem for Gaussians, which in the end results in

$$\begin{aligned} \mathbf{C_y} \quad &= \quad |\theta_1|\mathbf{C_x} + 2|\theta_2|^2 \mathbf{C_x} \circ |\mathbf{C_x}|^2 \\ &+ \quad 2\bar{\theta}_1\theta_2 \left(\mathbf{I}_{MN} \otimes \text{diag}(\mathbf{C}_{\mathbf{x}_n})\right) \mathbf{C_x} + 2\bar{\theta}_2\theta_1 \mathbf{C_x} \left(\mathbf{I}_{MN} \otimes \text{diag}(\mathbf{C}_{\mathbf{x}_n})\right) \\ &+ \quad 2|\theta_2|^2 \left(\mathbf{I}_{MN} \otimes \text{diag}(\mathbf{C}_{\mathbf{x}_n})\right) \times \mathbf{C_x} \left(\mathbf{I}_{MN} \otimes \text{diag}(\mathbf{C}_{\mathbf{x}_n})\right) \end{aligned} \tag{4.47}$$

where $\circ$ is the element-wise product. A full derivation of this can be found in [10].

4.6 OSCILLATOR PHASE NOISE

In the case of phase noise, formulating a stochastic model in the same format as for the power amplifier is not trivial as phase noise is in itself not generated through a nonlinear function but is in fact already

described as a stochastic process. Therefore, we may not use the same straightforward method using the Bussgang theorem. However, we may do a signal decomposition using LMMSE Estimation in order to formulate a model in the linear same format.

We recall that the behavioral model for the phase noise is described by

$$y[n] = x[n]e^{i\varphi[n]} \tag{4.48}$$

where $\varphi[n] = \lambda\varphi[n-1] + w[n]$. The stochastic model for the phase noise, in this case, is written as

$$\mathbf{x} = \mathbf{G}^{\text{PN}}\mathbf{w} + \mathbf{e}^{\text{PN}} \tag{4.49}$$

where

$$\mathbf{G}^{\text{PN}} = e^{-\frac{2\pi^2 f_c^2 t_s \kappa}{1-\lambda^2}}\mathbf{I}_{MN}. \tag{4.50}$$

In the case of phase noise with separate oscillators using PLL synchronization, the covariance of the error-term becomes

$$\mathbf{C}_{\mathbf{e}^{\text{PN}}} = \mathbf{C}_{\mathbf{y}} - e^{-\frac{4\pi^2 f_c^2 t_s \kappa}{1-\lambda^2}}\mathbf{C}_{\mathbf{x}} \tag{4.51}$$

in which the output covariance is

$$\mathbf{C}_{\mathbf{y}} = \text{diag}\left(\boldsymbol{\psi}\right)\text{diag}\left(\mathbf{C}_{\mathbf{x}}\right) + e^{-\frac{2\pi^2 f_c^2 t_s \kappa}{1-\lambda^2}}\text{nondiag}\left(\mathbf{C}_{\mathbf{x}}\right). \tag{4.52}$$

Here, $\boldsymbol{\psi} = \text{vec}\left(\left[\boldsymbol{\psi}_0, \ldots, \boldsymbol{\psi}_{N-1}\right]\right)$ which for each $\boldsymbol{\psi}_m$ may be computed as

$$\boldsymbol{\psi}_m = e^{-\frac{4\pi^2 f_c^2 t_s \kappa}{1-\lambda^2}\left(1-\lambda^{\left|(m+\frac{N}{2})\text{mod}N-\frac{N}{2}\right|}\right)}. \tag{4.53}$$

It is of interest to notice that the gain and covariance matrix depend only on PLL, the oscillator parameter λ, and κ.

4.7 STOCHASTIC MODELING OF DATA CONVERTERS

Finally, before moving on to concatenate the model-blocks into a complete transmitter model, we need a description of the quantization noise from the data converters. Just as with power amplifier distortion and phase noise, we model the process in a linear fashion. We have

$$\mathbf{x} \quad = \quad \mathbf{G}^{\text{DAC}}\mathbf{w} + \mathbf{e}^{\text{DAC}}. \tag{4.54}$$

The gain matrix for a DAC, denoted

$$\mathbf{G}^{\text{DAC}} = \mathbf{I}_{MN} \otimes \text{diag}\left(\mathbf{g}^{\text{DAC}}\right), \tag{4.55}$$

will element-wise be computed as [11]

$$\mathbf{g}^{\text{DAC}} = \frac{\Delta}{\sqrt{\pi}} \text{diag}\left(\mathbf{C}_{\mathbf{x}_n}\right)^{-\frac{1}{2}} \sum_{i=1}^{2^q-1} e^{-\Delta^2 (i-2^{q-1})^2 \left(\mathbf{C}_{\mathbf{x}_n}\right)^{-1}}. \tag{4.56}$$

Now again, following the orthogonality we get the error covariance matrix:

$$\mathbf{C}_{\mathbf{e}^{\text{DAC}}} = \mathbf{C}_{\mathbf{y}} - \mathbf{G}^{\text{DAC}} \mathbf{C}_{\mathbf{x}} \mathbf{G}^{\text{DAC}}. \tag{4.57}$$

The quantized output covariance matrix, from [11, Eq. 10], is then computed as

$$\begin{aligned} \mathbf{C}_{\mathbf{y}} \quad &\approx \quad \frac{\Delta^2}{2}(2^q-1)^2 \mathbf{I}_{BN} - 4\Delta^2 \sum_{i=1}^{2^q-1} \left(i - 2^{q-1}\right) \\ &\times \quad \Phi\left(\sqrt{2}\text{diag}\left(\mathbf{C}_{\mathbf{x}}\right)^{-\frac{1}{2}} \left(i - 2^{q-1}\right)\right) \\ &+ \quad \mathbf{G}^{\text{DAC}} \text{nondiag}\left(\mathbf{C}_{\mathbf{x}}\right) \mathbf{G}^{\text{DAC}}. \end{aligned} \tag{4.58}$$

With the individual models for each of the subsystem component, a more complete transmitter model may be assembled.

4.8 MODEL CONCATENATION AND SIMULATIONS

To assemble the chain forming a complete transmitter chain model, we may use the linear properties of each subsystem model to our advantage. If we consider the linear models for two different (vector) nonlinear systems

$$\begin{aligned} \mathbf{y}_1 &= \mathbf{G}_1 \mathbf{x} + \mathbf{e}_1 \\ \mathbf{y}_2 &= \mathbf{G}_2 \mathbf{x} + \mathbf{e}_2 \end{aligned} \tag{4.59}$$

the concatenated model for the series non-linearity becomes

$$\mathbf{y} = \mathbf{G}_2(\mathbf{G}_1 \mathbf{x} + \mathbf{e}_1) + \mathbf{e}_2. \tag{4.60}$$

Using this step repeatedly, we may find the transmitter-model as derived in [10]

$$\begin{aligned} \mathbf{y} &= \mathbf{G}^{\text{PA}} \left(\mathbf{G}^{\text{PN}} \left(\mathbf{G}^{\text{DAC}} \mathbf{z} + \mathbf{e}^{\text{DAC}}\right) + \mathbf{e}^{\text{PN}}\right) \mathbf{w} + \mathbf{e}^{\text{PA}} \\ &= \underbrace{\mathbf{G}^{\text{PA}} \mathbf{G}^{\text{PN}} \mathbf{G}^{\text{DAC}} \mathbf{z}}_{\text{Scaled and rotated signal}} + \underbrace{\mathbf{G}^{\text{PA}} \mathbf{G}^{\text{PN}} \mathbf{e}^{\text{DAC}} + \mathbf{G}^{\text{PA}} \mathbf{e}^{\text{PN}} + \mathbf{e}^{\text{PA}}}_{\text{Distortion noise}}, \end{aligned} \tag{4.61}$$

from which we may observe an equivalent gain matrix, $\mathbf{G}^{\text{PA}} \mathbf{G}^{\text{PN}} \mathbf{G}^{\text{DAC}}$ and an accumulative noise process with rescaled contributions from each subsystem component. Using the concatenated model, we may now describe the signal-to-interference, distortion and noise ratio (SINDR).

4.8.1 SIGNAL-TO-INTERFERENCE AND NOISE RATIO

As described in more detail in [10], the SINDR for an OFDM system at the kth UE and the lth subcarrier may be approximated by means of the concatenated model discussed in previous section. The SINDR is

$$\gamma_{k,l} \approx \frac{\exp\left(-\frac{2\pi f_c t_s \kappa}{1-\lambda^2}\right)\left|\hat{\mathbf{h}}_{k,l}^T \operatorname{diag}(\mathbf{g}^{\mathrm{PA}}) \operatorname{diag}(\mathbf{g}^{\mathrm{DAC}})\hat{\mathbf{p}}_{k,l}^T\right|^2}{I_{k,l}+E_{k,l}+N_0} \tag{4.62}$$

in which we have that

$$I_{k,l} = \exp\left(-\frac{2\pi f_c t_s \kappa}{1-\lambda^2}\right)\sum_{v\neq k}\left|\hat{\mathbf{h}}_{k,l}^T \operatorname{diag}(\mathbf{g}^{\mathrm{PA}}) \operatorname{diag}(\mathbf{g}^{\mathrm{DAC}})\hat{\mathbf{p}}_{v,l}^T\right|^2 \tag{4.63}$$

is the interference power and

$$\begin{aligned} E_{k,l} = \Bigg[&(\mathbf{F}_N \otimes \mathbf{I}_M)\left(\mathbf{G}^{\mathrm{PA}}\left(\exp\left(-\frac{2\pi f_c t_s \kappa}{1-\lambda^2}\right)\times\left(\mathbf{C}_{\mathbf{v}}-\mathbf{G}^{\mathrm{DAC}}\mathbf{C}_{\mathbf{z}}\mathbf{G}^{\mathrm{DAC}}\right)\right.\right. \\ &\left.\left.+\left(\mathbf{C}_{\mathbf{w}}-\exp\left(-\frac{2\pi f_c t_s \kappa}{1-\lambda^2}\right)\mathbf{C}_{\mathbf{v}}\right)\left(\mathbf{G}^{\mathrm{DAC}}\right)^H+\mathbf{C}_{\mathbf{x}}-\mathbf{G}^{\mathrm{DAC}}\mathbf{C}_{\mathbf{w}}\left(\mathbf{G}^{\mathrm{DAC}}\right)^H\right)\left(\mathbf{I}_M\otimes\mathbf{F}_N^H\right)\Bigg]_{k+lK,k+lK} \end{aligned} \tag{4.64}$$

is the received distortion power on the lth subcarrier and the kth user. Here, $\mathbf{F}_N$ is the $N \times N$ DFT-matrix for which $\mathbf{F}_N\mathbf{F}_N^H = \mathbf{I}_N$.

Looking at the interference power, comparing to conventional signal-to-interference-and-noise ratio (SINR)-analysis of massive MU-MIMO systems, further degeneration stemming from non-ideal hardware may be observed.

4.8.2 SIMULATIONS

In order to illustrate the usage of the stochastic transceiver model discussed in this chapter, we will present some basic link-simulations. These make use of the stochastic models in order to emulate an OFDM-based massive MU-MIMO array transmitter and we compare the results with simulations using conventional models. We will consider an OFDM-system with frequency selective linear precoding using maximum ratio transmission (MRT) and zero-forcing (ZF). The precoding matrices are defined as

$$\mathbf{P}_k^{\mathrm{MRT}} = \alpha_{\mathrm{MRT}}\frac{1}{M}\mathbf{H}_k^H \tag{4.65}$$

$$\mathbf{P}_k^{\mathrm{ZF}} = \alpha_{\mathrm{ZF}}\frac{1}{M}\mathbf{H}_k\left(\mathbf{H}_k\mathbf{H}_k^H\right)^{-1} \tag{4.66}$$

where

$$\mathbf{H}_k = \sum_{t=0}^{T}\hat{\mathbf{H}}_t e^{-jk\frac{2\pi}{N}t} \tag{4.67}$$

is the $M \times K$ frequency-domain matrix describing the channel at subcarrier k. α_{MRT} and α_{ZF} are chosen such that $\mathbb{E}\left[|\mathbf{x}_n|^2\right] = 1$ for the precoded vector $\mathbf{x}_n$. The full set of parameters are found in Table 4.2. We consider an OFDM-based MU-MIMO system with M antennas and K users and a Rayleigh inde-

Table 4.2 Simulation parameters

Parameter	**Setting**
Carrier frequency	3 GHz
Carrier type	OFDM
Number of occupied subcarriers	1200
FFT size	4096
Carrier bandwidth	20 MHz
Channel parameter	**Setting**
Channel type	Rayleigh IID in spherical coordinates
Number of channel taps	5
Power delay profile	Exponential
DAC parameter	**Setting**
q	6 bits
LSB (Δ)	0.0081
Phase-noise parameter	**Setting**
λ	0.99
κ	$5 \cdot 10^{-17}$
Power amplifier parameter	**Setting**
θ_1	1
θ_2	$-0.03491 + \mathrm{i}0.00565$

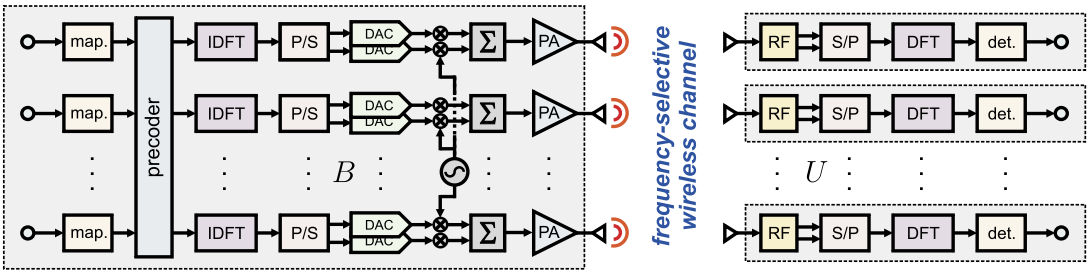

FIGURE 4.14

Complex baseband system model. The complex baseband system model including a base-station equipped with M antennas, each consisting of DAC's, local oscillators and power amplifiers. This is followed by the radio channel and K served users.

pendent identically distributed (IID) channel. Fig. 4.14 shows the system model including impairment models for quantization noise, phase noise and power amplifier distortion.

4.8.3 SIMULATION RESULTS

The simulation results are summarized in Figs. 4.15–4.17. Fig. 4.15 shows the simulated power spectral density of each model block as well as the composite transmitter model, compared to the corresponding

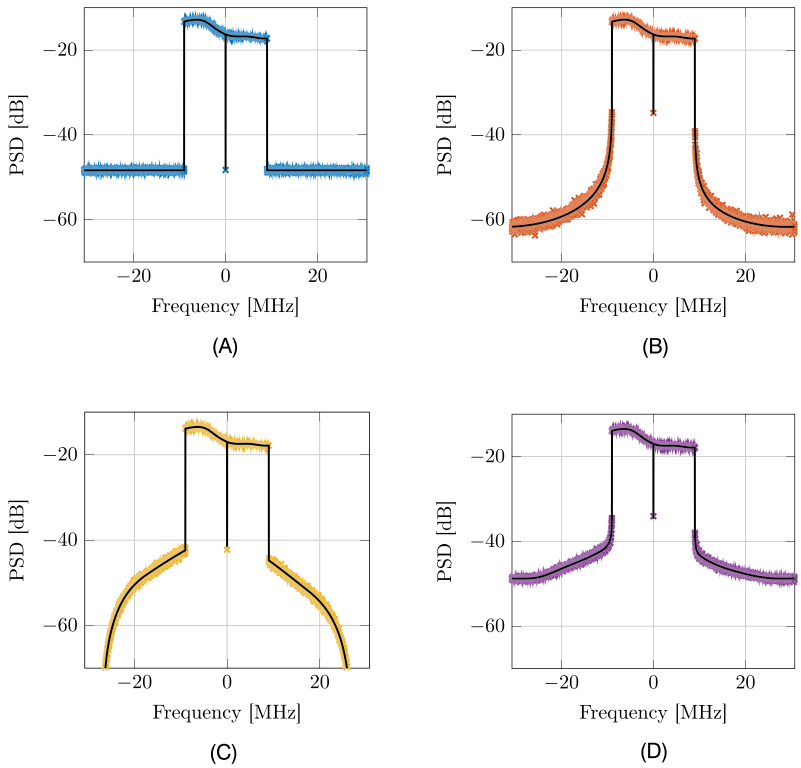

FIGURE 4.15

Output power spectral density from the statistical models. PSD of the transmitted signal for the case when each hardware impairment in the RF-chain are considered separately, and when all of the hardware impairments are considered together. The markers correspond to simulation results whereas the black lines are the analytical outcome. (A) Finite-resolution DACs only (ideal LO and linear PA). (B) Nonideal LO only (infinite-resolution DAC and linear PA). (C) Nonlinear PAs only (infinite-resolution DACs and ideal LO). (D) Concatenated impairment model (finite-resolution DACs, nonideal LO, and nonlinear PA).

behavioral models. As may be seen, the stochastic model accurately predicts the power spectral density in not only each model block, but also in the case of the complete transmit model. The PSD is accurately predicted both in- and out-of band, which is otherwise not the case for most linear and stochastic models which today is widely used in the literature, [3].

Fig. 4.16 shows the radiated power of both the transmit signal (A) and the adjacent channel power (B). Here we may spot similar effects to those noted in Section 4.1.5. In a similar manner, the inband distortion takes on a similar radiation pattern as the transmit signal in this case.

Finally, Fig. 4.17 shows the performance in terms of uncoded BER with and without impairment models. As may be observed, the radio hardware impairments has a negative impact on the uncoded BER performance for both ZF and MRT.

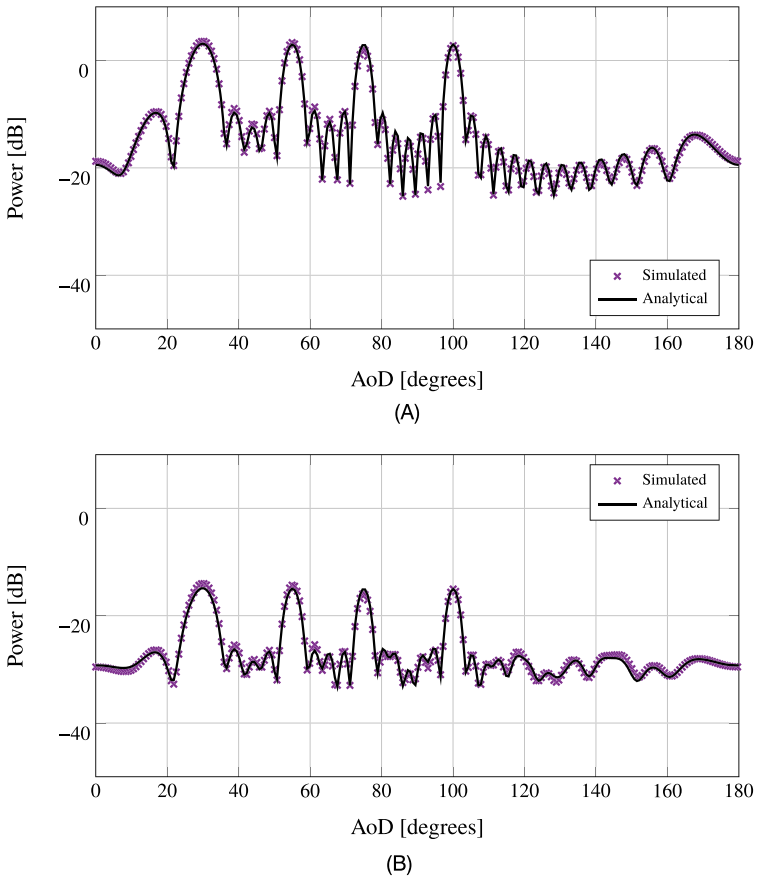

FIGURE 4.16

Simulated radiation patterns using stochastic impairment models. Simulated radiation patterns of the desired signal (A) and the impairment component (B), consisting of power amplifier distortion, phase noise, and quantization noise.

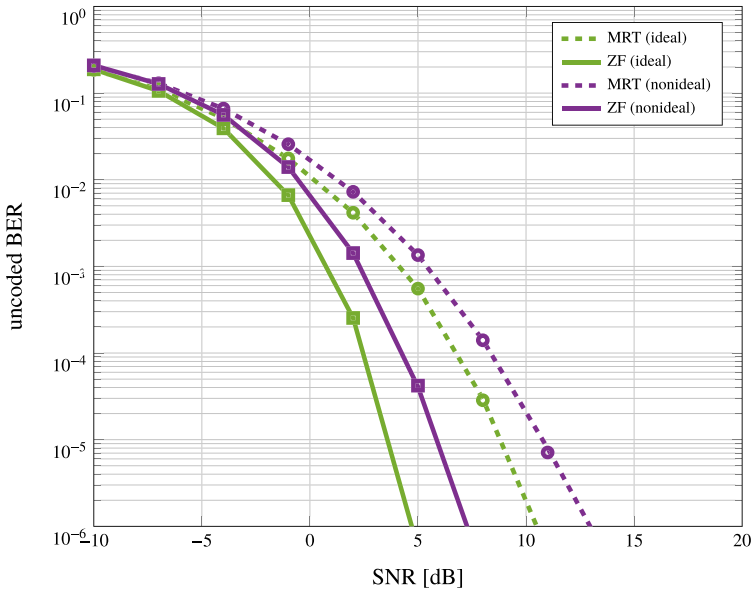

FIGURE 4.17

Link-performance assessment using stochastic impairment models. Comparison of uncoded BER using linear precoding, with and without the impact of hardware impairments.

REFERENCES

[1] S. Afsardoost, T. Eriksson, C. Fager, Digital predistortion using a vector-switched model, IEEE Transactions on Microwave Theory and Techniques (ISSN 0018-9480) 60 (4) (2012, April) 1166–1174, https://doi.org/10.1109/TMTT.2012.2184295.

[2] S. Benedetto, E. Biglieri, R. Daffara, Modeling and performance evaluation of nonlinear satellite links-a Volterra series approach, IEEE Transactions on Aerospace and Electronic Systems (ISSN 0018-9251) AES-15 (4) (1979, July) 494–507, https://doi.org/10.1109/TAES.1979.308734.

[3] E. Björnson, J. Hoydis, M. Kountouris, M. Debbah, Massive MIMO systems with non-ideal hardware: energy efficiency, estimation, and capacity limits, IEEE Transactions on Information Theory 60 (11) (2014) 7112–7139.

[4] N. Bjorsell, P. Suchánek, P. Handel, D. Ronnow, Measuring Volterra kernels of analog-to-digital converters using a stepped three-tone scan, IEEE Transactions on Instrumentation and Measurement 57 (4) (2008) 666–671.

[5] J.J. Bussgang, Crosscorrelation functions of amplitude-distorted gaussian signals, 1952.

[6] H. Chireix, High power outphasing modulation, Proceedings of the Institute of Radio Engineers (ISSN 0731-5996) 23 (11) (1935, Nov.) 1370–1392, https://doi.org/10.1109/JRPROC.1935.227299.

[7] L. Ding, G.T. Zhou, Effects of even-order nonlinear terms on predistortion linearization, in: Digital Signal Processing Workshop, 2002 and the 2nd Signal Processing Education Workshop. Proceedings of 2002 IEEE 10th, 2002, pp. 1–6.

[8] W.H. Doherty, A new high efficiency power amplifier for modulated waves, Proceedings of the Institute of Radio Engineers (ISSN 0731-5996) 24 (9) (1936, Sept.) 1163–1182, https://doi.org/10.1109/JRPROC.1936.228468.

[9] K. Hausmair, S. Gustafsson, C. Sánchez-Pérez, P.N. Landin, U. Gustavsson, T. Eriksson, C. Fager, Prediction of nonlinear distortion in wideband active antenna arrays, IEEE Transactions on Microwave Theory and Techniques (ISSN 1557-9670) 65 (11) (2017, Nov.) 4550–4563, https://doi.org/10.1109/TMTT.2017.2699962.

[10] S. Jacobsson, U. Gustavsson, D. Astely, G. Durisi, C. Studer, T. Eriksson, Modeling and analysis of transmit-RF impairments in massive MU-MIMO OFDM downlink, 2018, in preparation.

[11] S. Jacobsson, G. Durisi, M. Coldrey, C. Studer, Linear precoding with low-resolution DACs for massive MU-MIMO-OFDM downlink, CoRR, arXiv:1709.04846, http://arxiv.org/abs/1709.04846, 2017.

[12] J. Kim, K. Konstantinou, Digital predistortion of wideband signals based on power amplifier model with memory, Electronics Letters (ISSN 0013-5194) 37 (23) (2001, Nov.) 1417–1418, https://doi.org/10.1049/el:20010940.

[13] P.N. Landin, D. Rönnow, RF PA modeling considering odd–even and odd order polynomials, in: Communications and Vehicular Technology in the Benelux (SCVT), 2015 IEEE Symposium on, 2015, pp. 1–6.

[14] P.N. Landin, S. Gustafsson, C. Fager, T. Eriksson, Weblab: a web-based setup for PA digital predistortion and characterization [application notes], IEEE Microwave Magazine (ISSN 1527-3342) 16 (1) (2015, Feb.) 138–140, https://doi.org/10.1109/MMM.2014.2367857.

[15] P.M. Lavrador, T.R. Cunha, P.M. Cabral, J.C. Pedro, The linearity-efficiency compromise, IEEE Microwave Magazine (ISSN 1527-3342) 11 (5) (2010, Aug.) 44–58, https://doi.org/10.1109/MMM.2010.937100.

[16] D.B. Leeson, A simple model of feedback oscillator noise spectrum, Proceedings of the IEEE (ISSN 0018-9219) 54 (2) (1966, Feb.) 329–330, https://doi.org/10.1109/PROC.1966.4682.

[17] C. Mollén, U. Gustavsson, T. Eriksson, E.G. Larsson, Spatial characteristics of distortion radiated from antenna arrays with transceiver nonlinearities, IEEE Transactions on Wireless Communications (2018), accepted for publication, arXiv:1711.02439, http://arxiv.org/abs/1711.02439, 2017.

[18] C. Mollén, U. Gustavsson, T. Eriksson, E.G. Larsson, Out-of-band radiation measure for MIMO arrays with beamformed transmission, in: 2016 IEEE International Conference on Communications (ICC), 2016, May, pp. 1–6.

[19] G.E. Moore, Cramming more components onto integrated circuits, Electronics 38 (8) (1965) 114.

[20] D.R. Morgan, Z. Ma, J. Kim, M.G. Zierdt, J. Pastalan, A generalized memory polynomial model for digital predistortion of RF power amplifiers, IEEE Transactions on Signal Processing 54 (10) (2006) 3852–3860.

[21] I.S. Reed, On a moment theorem for complex Gaussian processes, IEEE Transactions on Information Theory 8 (3) (1962, Apr.) 194–195, https://doi.org/10.1109/TIT.1962.1057719.

[22] D. Root, et al., Polyharmonic distortion modeling, IEEE Microwave Magazine 7 (3) (2006) 44–57.

[23] A. Sripad, D. Snyder, A necessary and sufficient condition for quantization errors to be uniform and white, IEEE Transactions on Acoustics, Speech, and Signal Processing (ISSN 0096-3518) 25 (5) (1977, Oct.) 442–448, https://doi.org/10.1109/TASSP.1977.1162977.

[24] V. Volterra, Sopra le funzioni che dipendono da altre funzioni, Tip. della R. Accademia dei Lincei, 1887.

[25] B. Widrow, I. Kollár, Quantization Noise: Roundoff Error in Digital Computation, Signal Processing, Control, and Communications, Cambridge University Press, Cambridge, UK, ISBN 9780521886710, 2008.

[26] P. Zetterberg, A. Wolfgang, A. Westlund, et al., Initial multi-node and antenna transmitter and receiver architectures and schemes, mmMAGIC Deliverale D5.1, 2016.